Jansen, M. J. F., Gunter, B. C., Kusche, J. (2009): The impact of GRACE, GPS and OBP data on estimates of global mass redistribution. - Geophysical Journal International, 177, 1, pp. 1—13.

DOI: http://doi.org/10.1111/j.1365-246X.2008.04031.x doi: 10.1111/j.1365-246X.2008.04031.x

The impact of GRACE, GPS and OBP data on estimates of global mass redistribution

M. J. F. Jansen,[1] B. C. Gunter[1] and J. Kusche[2]

[1]*Delft Institute of Earth Observation and Space Systems(DEOS), Delft University of Technology, Delft, The Netherlands. E-mail: M.J.F.Jansen@tudelft.nl*
[2]*Helmholtz Centre Potsdam, GFZ German Research, Centre for Geosciences, Section* 1.3: *Gravity Field and Gravimetry, Telegrafenberg,* D-14473 *Potsdam, Germany*

Accepted 2008 October 22. Received 2008 October 20; in original form 2008 June 6

SUMMARY

In an effort to improve the estimates of global surface mass variations, an approach has been developed in which monthly gravity fields from the Gravity Recovery and Climate Experiment (GRACE) are combined with Global Positioning System (GPS) site displacements and modelled ocean bottom pressure (OBP) data. The motivation for this combination stems from the notion that while GRACE monthly fields provide excellent results for the mid- to high-degree spherical harmonics coefficients, they are currently unable to determine the lowest degree coefficients as accurately. In addition, the GRACE monthly fields do not deliver estimates of the geocentre motion (i.e. degree 1 terms), which are needed when comparing GRACE solutions with ground-based measurements. These ground-based measurements are normally given in a reference frame whose centre of mass does not coincide with the centre of mass of the whole earth system, resulting in non-zero degree 1 coefficients. Through loading theory, large-scale mass variations can be derived from globally distributed GPS site displacement vectors and modelled OBP values; however, both measurement types have their own limitations and do not have homogeneous coverage over the globe. To assess the impact that these errors would have on current and future real-data combinations with GRACE monthly fields, a sensitivity study was conducted. A range of combinations were explored in which the spatial distribution and quality of the GPS and OBP data sets were varied. The results show that significant improvements to the GRACE monthly gravity fields, in particular at the low degrees, can be achieved when these solutions are combined with present-day GPS and OBP products. An idealized scenario was also investigated to identify the specific shortcomings and limitations of a real data combination scenario. A description of the methodology, assessment criteria and results of the sensitivity study will be presented, along with a discussion of the overall findings and future potential of this work.

Key words: Inverse theory; Spatial analysis; Satellite geodesy; Time variable gravity; Global change from geodesy; Hydrology.

1 INTRODUCTION

The Gravity Recovery and Climate Experiment (GRACE) (Tapley *et al.* 2004) has provided the scientific community with a new way of observing the global distribution of mass over time. It has allowed large-scale mass transport processes, such as continental hydrology and polar ice mass changes, to be observed with unprecedented accuracy and at timescales of one month or less. Despite these advances, there are still some improvements to be gained by combining GRACE with other data sets. All satellite missions have their limitations, and for GRACE, these include reduced ground-track coverage near the equator and the insensitivity to degree one harmonics. It is known that GRACE is also less sensitive to the longest wavelength gravity signals, in particular those related to the Earth's oblateness (i.e. the $C_{2,0}$ harmonic). It has already been suggested that by incorporating other data sets, such as ocean bottom pressure (OBP) data derived from ocean models (Wu *et al.* 2006; Swenson *et al.* 2008) and GPS site displacements (Blewitt & Clarke 2003; Kusche & Schrama 2005; Lavallée *et al.* 2006), some of these limitations can be significantly improved. It should be noted that the GPS and modelled OBP data (further addressed here as simply OBP data) have limitations as well, primarily with reference to their spatial distribution over the globe.

Although it has already been recognized that the combination of these data sets would be helpful, the actual level of improvements that might be realized is still a matter of debate. The answer to this question is the focus of this study. We wanted to quantify the improvements that could be made to monthly mass distribution estimates when both realistic and idealized GPS and OBP data sets were utilized. In addition, we wanted to determine what the individual contribution of each data set would be to the total estimation. A sensitivity study of this nature cannot be done with real data alone; so, a range of simulations were created to explore the various facets of the data combinations. Properties of the real data, such as error characteristics, were still used in the simulated data to allow for a more realistic evaluation of the combinations. By working in the world of simulation, the exact contribution of each data set can be determined, issues surrounding data redundancy can be investigated and new scenarios can be explored for a hypothetical future data network. In short, all parameters can be varied, including the location, frequency and accuracy of the involved data sets. In the end, the idealized simulation results were compared with solutions computed from publicly available data products to evaluate the performance of current real-data combinations.

As will be shown, the results were encouraging and demonstrate that there is still significant improvement to be gained through the combination of multiple data sets with GRACE. The most notable improvements were in the determination of the low degree harmonics, including degree one terms (geocentre motion) and $C_{2,0}$. The OBP data proved to be more influential than the GPS data in terms of overall contribution, but the GPS data were useful for filling in sizeable gaps left by the OBP data over the continents.

This paper will contribute to the general understanding of global mass redistribution by providing a comprehensive analysis of the value and limitations to be expected from the combination of GRACE, GPS and OBP data. Some of the key findings include:

(1) An assessment of the improved observability of the total global mass redistribution signal (i.e. through degree and order 30) expected by the combination of the three data sets when compared to the GRACE-only solutions.

(2) An assessment of the expected improvement in the determination of $C_{2,0}$ (oblateness) resulting from the combination. This, in turn, highlights the improvements expected in the estimation of the mass redistribution signal surrounding the lower latitudes (equatorial).

(3) A demonstration of the stabilized estimation of the degree 1 terms (i.e. geocentre motion) that are a direct result of the combined solutions.

(4) These simulations will provide a better understanding of the strength of the combination process for current real-data inversions. As such, the simulations set the groundwork for future real-data combinations by providing valuable analysis of the data sets involved.

(5) The sensitivity study will also serve to highlight those regions that will have higher uncertainties and which could benefit from additional stations or improved *in situ* measurements.

The results of this study have relevance to a number of applications within the Earth sciences. When the recommendations of this study are eventually realized in a time-series of real-data combinations, the expected improvements to the degree one estimates will be valuable to any application that relies on the comparison of gridded data sets in an Earth-fixed reference frame (Dong *et al.* 1997; Chambers *et al*. 2007; Munekane 2007), such as ocean mass variability or polar mass balance studies. The improvements of the GPS and OBP data sets to the longer wavelengths will have a significant impact on the variable mass redistribution estimates. This in itself has implications to the broad topic of global climate change studies. Finally, the study highlights which regions would benefit most from future OBP data or GPS *in situ* measurements.

This paper will first provide a detailed description of the methodology behind the sensitivity study, including any assumptions that went into the simulated data sets, as well as the criteria used for evaluation. A number of case studies will be presented, which are designed to highlight the key conclusions of the sensitivity study. These include combinations of idealistic as well as realistic type data sets at varying degrees of resolution (i.e. the degree and order of the solutions). The optimal combinations obtained will be used to support the final conclusions of the analysis, including recommendations for future work.

2 METHODOLOGY

When combining different data sets, one has to decide how the information available will be represented and compared. The sections below highlight the specific choices made for this study, and include descriptions of the parametrization of the various surface mass loading solutions, how they were computed; and which criteria were used to evaluate the performance of the solutions.

2.1 Spherical harmonics and loading theory

All data sets used in this study incorporated globally distributed measurements that could be translated (analytically) into anomalies of a load distribution at the Earth's surface. As such, the use of spherical harmonics was the natural choice to represent the data sets. The benefit of this technique is that it allows for both the conservation of mass in the solutions, as well as control over the maximum surface resolution that could be fit to the data. This latter point is important since some of the data combinations performed for this study could not be solved for at the same resolution as others, a useful indication of the spatial limitations for certain combinations. As a brief summary of the technique, it can be shown (Wahr *et al.* 1998) that a mass distribution within a thin layer, $\Delta\sigma$, surrounding the Earth's surface can be represented by

$$\Delta\sigma(\lambda,\phi) = a\rho_{\mathrm{w}} \sum_{l=0}^{L} \sum_{m=0}^{l} \left[C^{\sigma}_{lm} Y^{\mathrm{C}}_{lm}(\lambda,\phi) + S^{\sigma}_{lm} Y^{\mathrm{S}}_{lm}(\lambda,\phi) \right], \tag{1}$$

where Y_{lm} are the fully normalized spherical harmonics and the superscript $^{\mathrm{C,S}}$ stands for cosine or sine. The indices l, m represent the degree and order of the spherical harmonics, with the maximum degree of the solution given by L. The arguments λ and ϕ are the spherical coordinates given in longitude and latitude, respectively. The variables C^{σ}_{lm}, S^{σ}_{lm} are the spherical harmonic coefficients for surface mass loading, given in dimensionless quantities. The mean radius of the Earth is represented by a, and ρ_{w} is the density of water (1025 $\mathrm{kg\,m^{-3}}$ in this study). It is important to note that this representation is only valid for a thin layer at the surface of the Earth, a reasonable assumption in this case since we are dealing with mass variations by water transport and because we assume that other variations are already removed in the data processing.

The GRACE, GPS and OBP data sets can all be used to evaluate the time variable loading forces acting on the Earth. Loading can be related to geoid change and vertical and lateral displacements of the Earth through a model. The Earth model used here is represented by the elastic loading Love-numbers of Farrell (1972). These loading Love-numbers are only degree-dependent and do not include the time-dependent viscous component, as the loading considered here is of a short timescale. The anisotropic behaviour of the Earth has only a small effect over the isotropic Earth model used in this study (Metivier *et al.* 2005). Spherical harmonic coefficients for geoid change, vertical and lateral displacement are given by Wahr *et al.*

(1998) and Blewitt & Clarke (2003)

$$C^{\mathrm{g}}_{lm} = \frac{3\rho_{\mathrm{w}}}{\rho_{\mathrm{e}}} \frac{(1 + k'_l)}{2l + 1} C^{\sigma}_{lm}, \tag{2}$$

$$C^{\mathrm{h}}_{lm} = \frac{3\rho_{\mathrm{w}}}{\rho_{\mathrm{e}}} \frac{h'_l}{2l + 1} C^{\sigma}_{lm}, \tag{3}$$

$$C^{\psi}_{lm} = \frac{3\rho_{w}}{\rho_{\mathrm{e}}} \frac{l'_l}{2l + 1} C^{\sigma}_{lm}, \tag{4}$$

where ρ_{e} is the average density of the Earth (5517 kg m^{-3} in this study) and k'_l, h'_l and l'_l are the elastic loading Love-numbers for gravitation, vertical displacement and lateral displacement, respectively. The indices on the spherical harmonic coefficients state that they represent the geoid (g),height (h),lateral movement (ψ). It should be noted that the degree 1 loading Love-numbers are dependent on the chosen reference system (Blewitt 2003).

2.2 The least-squares method

The various simulated solutions generated as part of this study assume the use of a standard normal equation approach with a Gauss–Markov model for each data set:

$$\mathbf{y} + \mathbf{e} = \mathbf{A}\mathbf{x}, \quad \mathbf{E}\{\mathbf{e}\} = \mathbf{0}, \quad \mathbf{D}\{\mathbf{e}\} = \mathbf{R}, \tag{5}$$

with observations collected in $\mathbf{y}$, stochastic residuals $\mathbf{e}$ and the variance covariance matrix for the measurement in $\mathbf{R}$. The operators $\mathbf{E}\{\}$ and $\mathbf{D}\{\}$ stand for the expectation and the dispersion, respectively. The individual least-squares solution of this model is

$$\mathbf{A}^T\mathbf{R}^{-1}\mathbf{A}\hat{\mathbf{x}} = \mathbf{A}^T\mathbf{R}^{-1}\mathbf{y}, \tag{6}$$

where $\mathbf{A}^T\mathbf{R}^{-1}\mathbf{A}$ is the normal matrix ($\mathbf{N}$) and the inverse of this matrix is the covariance matrix associated with the solution vector $\hat{\mathbf{x}}$. The solution vector will contain the spherical harmonic coefficients (C^{σ}_{lm}, S^{σ}_{lm}) and additional parameters depending on the data set. Each data set has its own solution space, meaning that the variables that can be estimated by each data set are not necessarily the same. For instance, the GRACE solutions are not sensitive to degree one coefficients, whereas the GPS and OBP data sets can estimate them. To solve the variables in the combination, a 'local' and 'global' parameter scheme is applied. In this scheme, the global parameters are estimated using all data sets in the combination, whereas the local parameters are estimated using only a specific data set. Prior to the combination, the normal matrix of the global parameters is adjusted to account for the local parameters following Reigber (1989):

$$\bar{\mathbf{N}}_{\mathrm{g}} = \mathbf{N}_{\mathrm{g}} - \mathbf{N}^T_{\mathrm{lg}}\mathbf{N}^{-1}_{\mathrm{l}}\mathbf{N}_{\mathrm{lg}}. \tag{7}$$

Where $\mathbf{N}_{\mathrm{g}}$ is the part of the normal matrix associated with the global parameters. $\mathbf{N}_{\mathrm{l}}$ is the part of the normal matrix belonging to the local parameters. $\mathbf{N}_{\mathrm{lg}}$ is the part of the normal matrix that represents the correlations between the local and global parameters. After creating the global normal equation matrix, the covariance matrix for the global parameters, $\mathbf{Q}_{\mathrm{g}}$, is easily generated through a matrix inversion. The covariance matrix for the local parameters, $\mathbf{Q}_{\mathrm{l}}$, can be computed by the following

$$\mathbf{Q}_{\mathrm{l}} = \mathbf{N}^{-1}_{\mathrm{l}} + \mathbf{N}^{-1}_{\mathrm{l}}\mathbf{N}_{\mathrm{lg}}\bar{\mathbf{N}}^{-1}_{\mathrm{g}}\mathbf{N}^T_{\mathrm{lg}}\mathbf{N}^{-1}_{\mathrm{l}}. \tag{8}$$

The covariances between the local and global parameters after the combination can be acquired by

$$\mathbf{Q}_{\mathrm{lg}} = -\mathbf{N}^{-1}_{\mathrm{l}}\mathbf{N}_{\mathrm{lg}}\bar{\mathbf{N}}^{-1}_{\mathrm{g}}. \tag{9}$$

In this way, the full covariance matrix of a single data set can be reconstructed after the combination.

2.3 Ideal to real scenarios

One of the many objectives of this study was to explore the effect that gaps and irregularities in the data distribution of the OBP and GPS data sets have on the quality of the combined solutions. To better understand the impact of these factors, a series of hypothetical test cases were developed, which each had a different global distribution of data points. The spatial distribution of these data points ranged from an idealistic dense and homogeneous case to a scenario that closely resembles the current real data networks. The ideal cases were generated by taking an icosahedron and projecting the computed vertexes onto the sphere, resulting in a set of 12 points that are perfectly equidistant from each other. To generate more points on the sphere, the faces of the icosahedron were then subdivided into smaller triangles until the desired amount of points were obtained. As the generated vertexes on the icosahedron faces are projected onto a sphere, the subpoints are not perfectly equidistant any more. The number of points, n, that can be generated by this method is given by $n = 10f^2 + 2$, where f is the frequency of the subdivision. This frequency is different for the two data sets: for the GPS data sets, the number of generated points over land are close to the amount of stations seen in real world GPS networks($\approx$180), and likewise, for the OBP data sets, the number of points over the ocean are approximately the same as the amount of gridpoints provided in real world OBP grids($\approx$1450 for a $5^\circ \times 5^\circ$ grid). What we term the 'ideal' cases for the GPS and OBP data sets is illustrated at the top of Fig. 1.

The ideal cases are clearly not realistic as they assume that the number of GPS data points has the same density of points over the oceans (likewise for the ideal OBP case over land). As a result, an intermediate distribution was generated using the homogeneously distributed measurements and masking out unrealistic data, such as points over the ocean for the GPS network and points over land for the OBP grid, to generate an extra case which we term the 'semi-ideal' case. This case is also shown in Fig. 1.

A third and final distribution of data points was chosen to reflect the current real-data distribution of stations and gridpoints for the GPS and OBP data. For the GPS data, this 'real-data' case was modelled after the station network of the International GNSS Service (IGS). For the OBP data, the real-data case emulated the Estimation of the Circulation and Climate of the Ocean (ECCO; Stammer *et al.* 2002) models, which are publicly available ocean circulation models that provides OBP information on various grid sizes. Both of these cases are illustrated at the bottom of Fig. 1, where the OBP data is given on a $5^\circ \times 5^\circ$ grid. It is clear from looking at Fig. 1 that the distribution of points between the ideal/semi-ideal and the real-data cases is substantial, particularly for the GPS case; however, the three cases are useful for determining the overall potential of a given data set. For example, if the contribution of the GPS data can be shown to increase significantly with a data distribution more closely resembling the ideal cases, then this might provide incentive for expanding the IGS network to areas with sparse coverage.

2.4 Sensitivity tools

When the GRACE, GPS and OBP data sets were combined in the various simulations, it was useful to know which of these data sets were contributing the most to the solution. More specifically, we

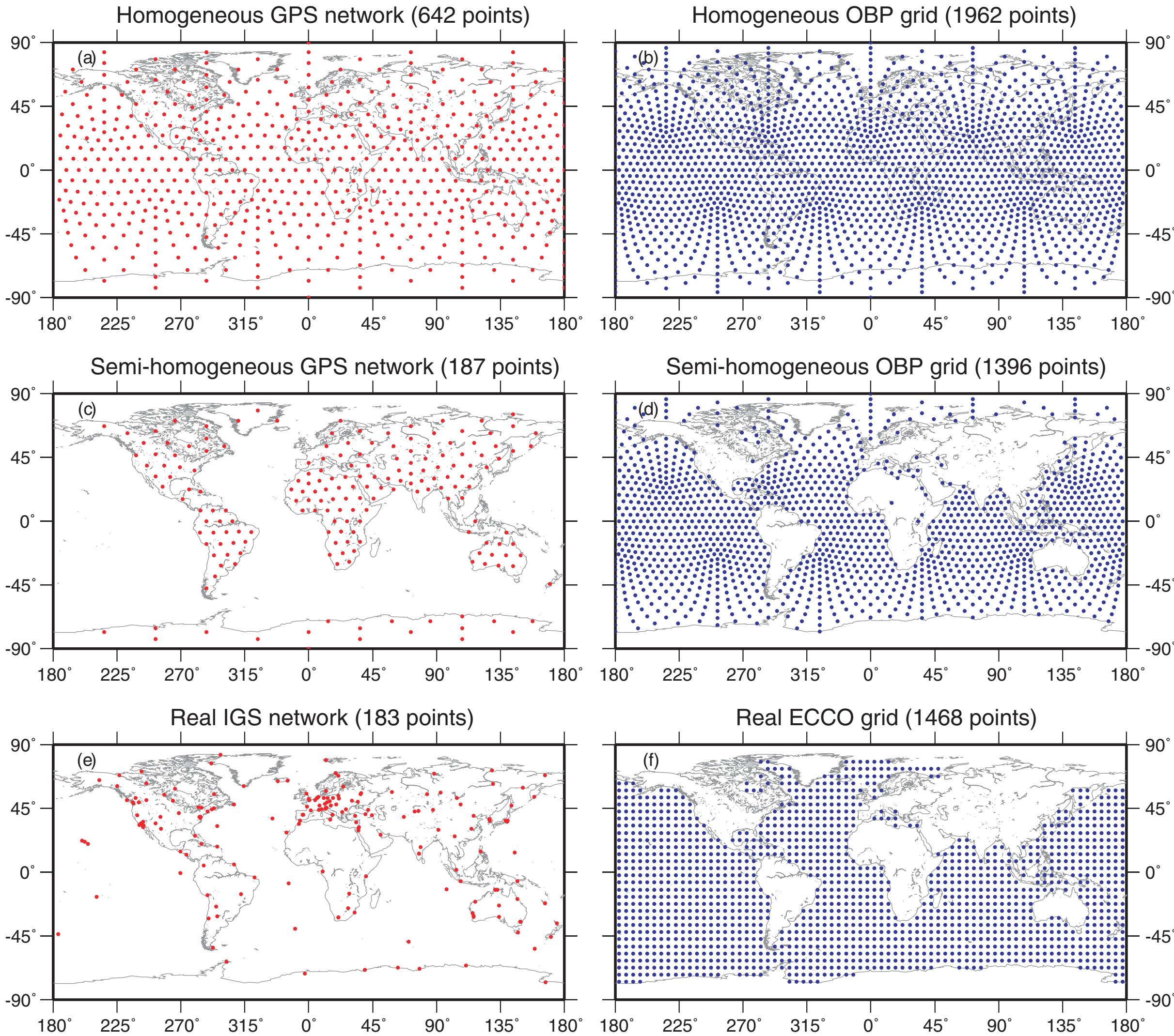

Figure 1. The global distribution of the different scenarios for GPS(left-hand panel) and OBP(right-hand panel). The top row gives the distributions for the ideal scenario (homogeneous distribution). The middle row shows the semi-ideal scenario (homogeneous over land or ocean). The bottom row shows the real-type scenario (IGS and ECCO).

were interested in the contribution of each data set at the level of individual harmonic coefficients. This was done to see if certain data sources contributed more than others to the estimation of specific regions (i.e. the long or short wavelength signals) of the load distribution spectrum. To determine these specific contributions, the following quantity was computed,

$$\mathbf{c}^{(i)} = \mathrm{diag}\Big(\big[\bar{\mathbf{N}}^{(i+j)}\big]^{-1}\bar{\mathbf{N}}^{(i)}\Big), \tag{10}$$

where $\bar{\mathbf{N}}^{(i)}$ is the normal matrix of data set i, and $\bar{\mathbf{N}}^{(i+j)}$ the combined normal matrix of two data sets. The inverse of the latter matrix can be composed by the use of eqs (8) and (9) and the covariance of the combined global parameters. The functional diag() represents the diagonal of the input matrix. The resulting value, $\mathbf{c}^{(i)}$, is then the percentage contribution of the individual data set to the total estimated value of the coefficient.

In addition to evaluating the contributions of the data set to the determination of the coefficient value, it is also valuable to look at the formal errors. The reduction of the formal error achieved by adding data set (j) to data set (i) is given by,

$$r_k^{(j)} = \frac{\hat{\sigma}_k^{(i)} - \hat{\sigma}_k^{(i+j)}}{\hat{\sigma}_k^{(i)}}, \tag{11}$$

where $\hat{\sigma}_k$ is the standard deviation of the estimated parameter k, derived from the covariance matrix. The resulting value, $r_k^{(j)}$, describes the percentage that the formal error drops by adding a data set to the final combination.

The final evaluation tool computes the formal error improvement of a regional mean. The standard deviation of such a regional mean can be calculated by the following:

$$\hat{\sigma}^2_{(\mathrm{region})} = \mathbf{s}^T_{(\mathrm{region})}\bar{\mathbf{N}}^{-1}\mathbf{s}_{(\mathrm{region})}, \tag{12}$$

where $\mathbf{s}_{(\mathrm{region})}$ is the vector that holds the normalized spherical harmonic coefficients of a region function (Wahr *et al.* 1998). Such a region function is one inside the region and zero outside. The $\hat{\sigma}_{(\mathrm{region})}$ can be used in eq. (11) to calculate the improvement of a particular region, such as an ocean or continental river basin.

3 DATA SETS

In this section, we provide a brief overview of the various data sets that went into the sensitivity study. Of primary concern is the treatment of the *a priori* errors associated with each data set, as well as how they were utilized in the combinations.

3.1 GRACE monthly gravity fields

The publicly available GRACE monthly solutions are provided in terms of spherical harmonic coefficients of the gravitational potential. The solutions also provide information regarding the formal and calibrated standard deviations of these coefficients.

The GRACE potential coefficients were used in this study by first transforming them into variations of geoid heights, given by

$$\Delta N(\lambda, \phi) = a \sum_{l=2}^{L} \sum_{m=0}^{l} \left[C_{lm}^{\mathrm{g}} Y_{lm}^{\mathrm{C}}(\lambda, \phi) + S_{lm}^{\mathrm{g}} Y_{lm}^{\mathrm{S}}(\lambda, \phi) \right], \tag{13}$$

and then into monthly loading through the method described earlier in eq. (2). The same transformation must be applied to the normal matrix before it can be used in the combination. This normal matrix is typically not provided as part of the public distribution of the monthly gravity solutions; however, the Center for Space Research (CSR) was able to provide this study with two complete RL04 covariance matrices. These covariance matrices extended to degree and order 60 and were calibrated to represent what the true errors in the solutions are believed to be. The two covariance matrices were from the months of 2004 September and 2006 August and, in terms of solution quality, represent the high and low end of the spectrum for the CSR RL04 solutions. These two months were specifically requested to evaluate the performance of the combined solutions when the accuracy of the GRACE information varied. For example, the 2004 September solution was generated during a period when the GRACE satellites were in a near-repeat orbit track that significantly reduced the solution quality for that month (Klokočnik *et al.* 2008). Fig. 2 provides a comparison of the (square-root) degree variances of the standard deviations for the two covariance matrices provided, as well as the calibrated errors for all of the available CSR RL04 solutions from 2002 to 2007. The figure also highlights the increased error at the low (smaller than 7) and high (larger than 30) degrees, which is inherent to this type of satellite mission.

From the full covariance matrices, the normal equations can be easily formed through a simple matrix inversion. It is important to note that the solutions provided did not include degree one coefficients.

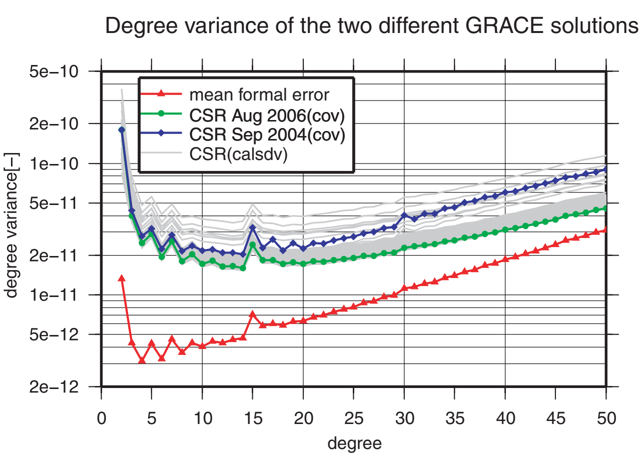

Figure 2. Degree variance plot of the monthly CSR RL04 GRACE solutions in unit of dimensionless gravitational potential. The standard deviation of the two calibrated covariance(cov) matrices provided by the CSR (blue & green) are plotted together with the calibrated standard deviations(calsdv) of all the available months (grey). Also the formal error averaged over all the months is shown (red) to illustrate the difference between formal and calibrated errors.

3.2 GPS station positions

The GPS station positions are provided as Cartesian coordinates in a global reference frame (e.g. ITRF2005). Displacements are computed by referencing these positions to a mean position and transforming them into a local height, east, north frame. By including hundreds of stations simultaneously, a displacement field can be expressed through a spherical harmonic expansion. Through the use of the relations (3) and (4), the loading can be retrieved from this displacement field. Together with the spherical harmonic coefficients, an additional 7-parameter set is estimated to account for potential non-linear offsets in the reference frame (i.e. residual Helmert transformation parameters). For combinations involving these GPS displacements, the spherical harmonic expansion began at degree one. These degree one coefficients represent the motion of the centre of mass of the Earth system with respect to the centre of figure, and in this paper, this will be called geocentre motion. To calculate the geocentre motion from the station displacements, the degree one loading Love-numbers corresponding to the centre of figure have to be used (Wu *et al.* 2002; Blewitt 2003). The following equations, together with eqs (3) and (4), describe the relationship between the GPS site displacements and the loading spherical harmonics in the presence of an additional 7-parameter transformation.

$$\Delta h = a \sum_{l=1}^{L} \sum_{m=0}^{l} \left[C_{lm}^{\mathrm{h}} Y_{lm}^{\mathrm{C}}(\lambda, \theta) + S_{lm}^{\mathrm{h}} Y_{lm}^{\mathrm{S}}(\lambda, \theta) \right] + \mathbf{e}_{\mathrm{h}} \cdot \Delta \mathbf{x} - a \Delta s, \tag{14}$$

$$\Delta x = a \sum_{l=1}^{L} \sum_{m=0}^{l} \left[C_{lm}^{\psi} \frac{\partial}{\partial \lambda} Y_{lm}^{\mathrm{C}}(\lambda, \theta) + S_{lm}^{\psi} \frac{\partial}{\partial \lambda} Y_{lm}^{\mathrm{S}}(\lambda, \theta) \right] + \mathbf{e}_x \cdot \Delta \mathbf{x} + \mathbf{e}_y \cdot \boldsymbol{\epsilon}, \tag{15}$$

$$\Delta y = a \sum_{l=1}^{L} \sum_{m=0}^{l} \left[- C_{lm}^{\psi} \frac{\partial}{\partial \theta} Y_{lm}^{\mathrm{C}}(\lambda, \theta) - S_{lm}^{\psi} \frac{\partial}{\partial \theta} Y_{lm}^{\mathrm{S}}(\lambda, \theta) \right] + \mathbf{e}_y \cdot \Delta \mathbf{x} + \mathbf{e}_x \cdot \boldsymbol{\epsilon}, \tag{16}$$

where Δh, Δx and Δy are the displacements of a station in height, east and north direction. The variables $\Delta \mathbf{x}$, Δs, $\boldsymbol{\epsilon}$ are the seven residual Helmert transformation parameters that translate, scale and rotate the reference system. These are added to resolve the small differences between realization of the reference system by the sparse GPS network and the true reference system. The argument θ is the colatitude, which is related to the latitude by $\theta = 90^\circ - \phi$.

As mentioned earlier, the real-data network used for the GPS data will be represented by a series of IGS weekly solutions, for which full covariance matrices of the site displacement estimates are publicly available. For the other GPS scenarios (ideal and semi-ideal), the error statistics of the IGS weekly solutions were used to provide a realistic error bound for the station coordinates of these hypothetical networks. This was done by neglecting station correlations (since these are not known in the ideal networks) and

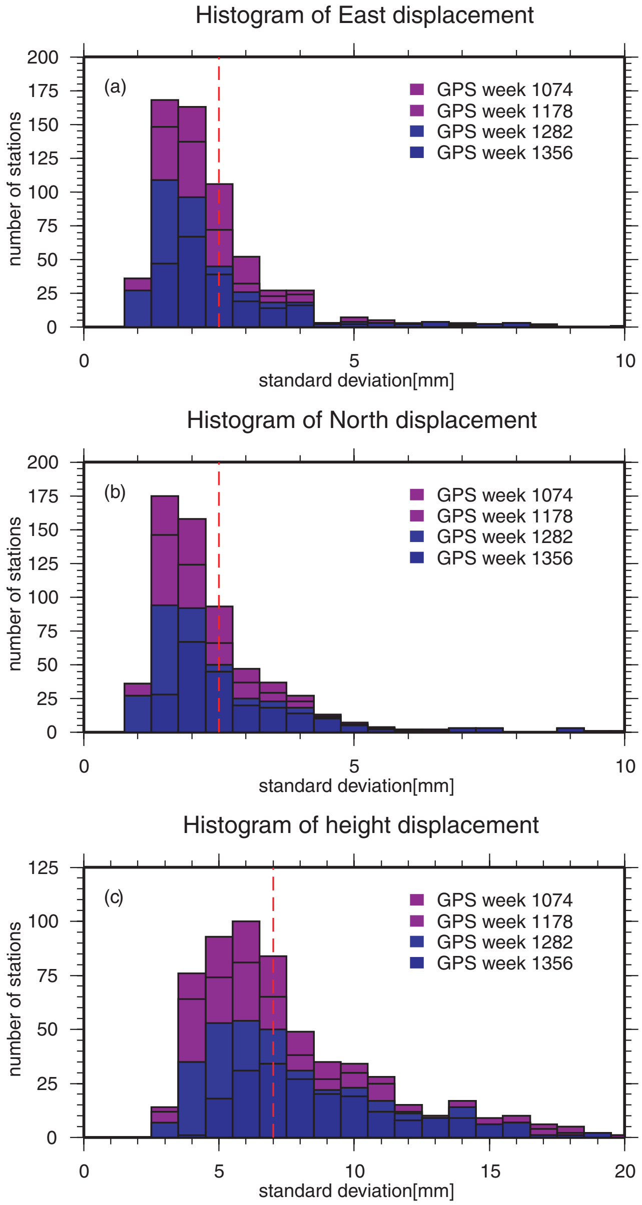

Figure 3. Histogram of the standard deviations of the three GPS station components. For the in-plane displacement (top two plots) the bin size is 0.5 mm, and for the out-of-plane displacement (bottom plot) the bin size is 1 mm. The dashed red lines represent the standard deviations used in this study for the ideal and semi-ideal scenarios.

looking only at the standard deviations per component. Fig. 3 gives the histograms for the standard deviations in the height, east and north component as computed from a randomly chosen set of four IGS covariance matrices. Based on these histograms, the standard deviation for the ideal and semi-ideal station distributions were chosen to be 7 mm for height displacement and 2.5 mm for lateral displacements. These values, indicated by the dashed vertical lines in Fig. 3, are relatively conservative error bounds with roughly 75 per cent of the IGS error estimates from the four weekly solutions falling below these levels for the lateral displacements and roughly 60 per cent for the height displacement. The lower percentage for the height displacement is justified due to the larger tail of the histogram.

3.3 Ocean bottom pressure models

OBP data sets are derived from time integrated models of ocean circulation. The OBP data give the sum of the water column above a particular point and are highly dependent on the sea surface heights. Measurements of the ocean's topography (via altimetry) are assimilated into these models, as well as density related data, wind and sea surface temperature; however, the estimation of errors in mass reproduction is extremely difficult, and as a result, most OBP data sets do not provide information regarding model uncertainties.

In a spherical harmonic expression, the variation of the OBP will be,

$$\Delta p(\lambda,\phi) = ag\rho_w \sum_{l=1}^{L}\sum_{m=0}^{l}\left[C^p_{lm}Y^C_{lm}(\lambda,\phi) + S^p_{lm}Y^S_{lm}(\lambda,\phi)\right] + W_{\text{offset}}, \tag{17}$$

where g is the average gravitation over the Earth's surface. The term W_{offset} is included to correct for the volume conservation of the ocean circulation models. This volume conservation could introduce a mass difference, that is, offset, between the OBP data and the other two data sets (Clarke *et al.* 2005). The W_{offset} can be expressed in spherical harmonics by introducing $C^p_{0,0}$, such that the summation over l in (17) will start at zero. The coefficients C^p_{lm}, S^p_{lm} are in the first approximation identical to the C^σ_{lm}, S^σ_{lm} coefficients, but start to differ when one takes into account the variation in gravitation over the Earth's surface.

The sea surface heights, which are assimilated into the ocean models, come from space-borne radar altimetry, such as Jason and TOPEX/Poseidon. Studies (Fukumori *et al.* 1999; Ponte *et al.* 2007) have shown that the sea surface height estimations from space-borne radar altimetry may be accurate to 3.0 cm for a 10 d repeat orbit on average. These studies also indicate that the accuracy of space-borne radar altimetry has a latitudinal dependence, but this effect is counteracted by the errors in the estimation of the steric component. There were several ocean circulation models available for use in this study; however, to limit the analysis, only the OBP models produced by ECCO were used. The ECCO models are given in regular grid cells, which can create resonance errors for certain spherical harmonics. These grid cells can have different sizes ranging from a $(1/8)^\circ$ to 1°, meaning that the models are interpolated between the ground-tracks of the satellite measurements. The TOPEX/Poseidon and Jason orbits repeat every 127 orbits, leaving a ground-track spacing of 2.8° on the equator. Therefore, we average the data to a 5° regular grid to minimize the effect of the modelling error. This also means that we represent the majority of the ECCO models, as the actual grid size of the ECCO model is not important and the error characteristics are derived from the data used by most models. For the ideal and semi-ideal cases, the grid spacing is taken to be as close to 5° as possible.

4 RESULTS

All three data sets that are used in this study have different temporal resolutions. For example, the GPS solutions are provided on a weekly basis, whereas the GRACE fields are typically released in monthly time frames. To overcome these temporal differences, the combined normal matrices are weighted; so, they represent the data available in the chosen time frame. Since the coverage and the temporal resolution for the GRACE solutions are related, simply weighting the normal matrix does not give a good estimate of a GRACE solution for a time frame that is different from a month. As a result, the normal matrices of the GPS and OBP data sets have to be weighted so that they will represent data that can be collected in one month. For these two data sets, the observations have a constant location in time and allows the weighting of the normal matrix to represent different time frames. For example, to correspond to the roughly four GPS weeks in one month, a scaling factor of 4 is applied to the GPS weekly solutions. In other words, the errors of the GPS solutions are divided by $\sqrt{4} = 2$. The error estimates for the OBP data sets are based on a 10 d repeat orbit, resulting in a scaling factor of 3 for the normal matrix. Hence, the errors of the OBP data sets are divided by $\sqrt{3} \approx 1.7$. The goal of this weighting scheme is to provide *a priori* error estimates of the GPS and OBP data, which more closely represent the error of a monthly average.

4.1 The Combination of GPS with OBP

As already discussed, by nature the GPS and OBP data sets have large gaps over the oceans or the continents. This will often result in poor or unstable solutions when attempting to estimate a high degree and order set of spherical harmonic coefficients. The cause is primarily the fact that the high degree and order coefficients cannot be estimated accurately from such sparse data sets. This creates large errors of omission and commission, which in turn alias into the lower degrees. To minimize these errors, regularization techniques are often employed (Blewitt & Clarke 2003; Kusche & Schrama 2005; Mendes Cerveira *et al.* 2006; Wu *et al.* 2006); however, this approach can lead to the introduction of biases to the solution. A natural alternative method is to combine the two data sets in the same least-squares process so that the gaps are minimized and no regularization is required. From the point networks shown earlier in Fig. 1, it is clear that the two data sets are quite complimentary in terms of their spatial distribution, making this option a reasonable choice. Using this second approach, a series of combinations were generated using the three different data distributions discussed earlier (ideal, semi-ideal and real-type), expanded to degree and order 20 (20×20). The contribution of the GPS component to the total solution for the various distributions is illustrated in Fig. 4, according to eq. (10).

Starting first with the ideal case, it was found that the GPS data contributed little to the total solution when only GPS and OBP were combined. The influence of the GPS data to the combination was limited primarily to the lower degrees. This can be explained by the decreasing nature of the loading Love-numbers, which gives the higher degrees a lower power. Other reasons include the sparse measurement distribution for GPS, together with the triple measurements per station (i.e. the lateral displacement measurements can be helpful for the resolution of the low degrees). What is important to note from Fig. 4(a) is that although the OBP data set overall has smaller errors with respect to the GPS data set, the lowest degrees are still improved slightly by the incorporation of GPS data.

When looking at the semi-ideal case, the contribution of the GPS measurements to the combination becomes much more significant. Still, the contribution of the GPS data is limited at higher degrees, for the same reasons that were explained in the previous paragraph. If the maximum degree of the combination is lowered, the contribution of the GPS measurement diminishes. This indicates that OBP data over the oceans is not sufficient to estimate up to 20×20, due to large correlations. Without filling the gaps, it is not possible to raise the resolution of the spherical harmonics to a level that would be sufficient to prevent spatial aliasing in the data-covered regions. This shows that the data gaps have a large influence on the solution

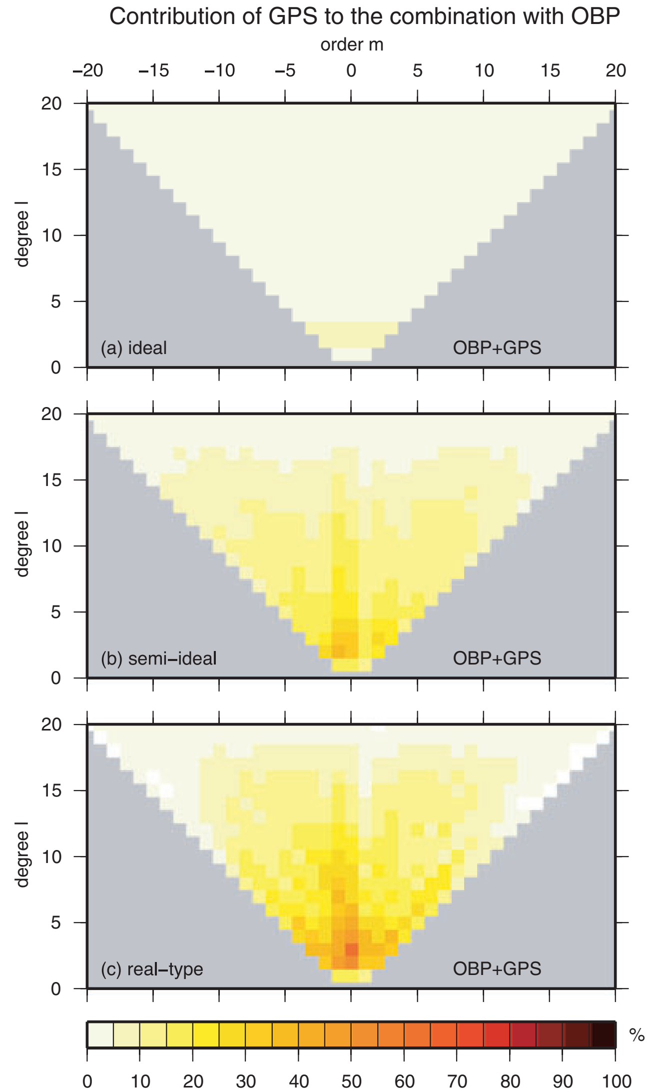

Figure 4. The contribution of GPS to a combination with OBP for the three scenarios. From top to bottom the scenarios are ideal, semi-ideal and real, respectively. The triangle plots represent the spherical harmonic coefficients, where positive orders are for the cosine coefficients and negative orders are for the sine coefficients.

and, by filling these gaps with other measurements, the results can be improved dramatically.

For the real case, the GPS measurements contribute even more to the solution than in the semi-ideal case. This is partially due to the small number of GPS stations distributed over the oceans (islands), which are not present in the semi-ideal case. Also, the extra gaps over the polar regions in the ECCO data will increase the contribution of the GPS data to the combination. A closer look at Fig. 4(c) shows that the contribution of GPS is now more focused around the zonals. This is due to the regular grid in which the ECCO data is given, resulting in more data per parallels. As seen for all cases, the GPS measurements mainly contribute to the lower degrees, with very little impact at the higher degrees.

Fig. 5 shows the global errors for a 10×10 combination of IGS and ECCO compared with the first 10 degrees of the 2006 August solution of GRACE. It highlights the small errors of the ECCO data set over the oceans, as well as the improved accuracy of the ECCO-IGS solution over the poles. The point of the plot is to visualize the

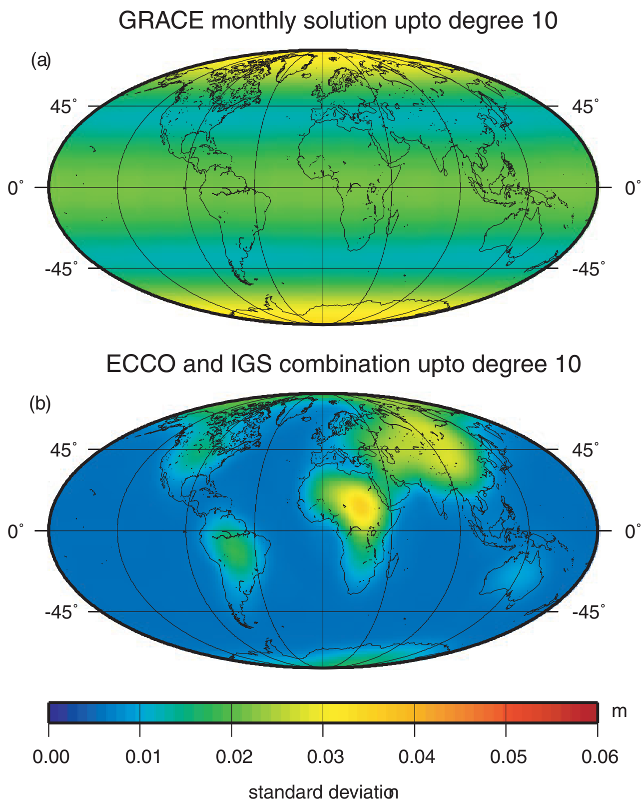

Figure 5. The standard deviation of GRACE and the ECCO-IGS combination projected onto the Earth's surface. The top plot shows the standard deviation of GRACE (2006 August) and the bottom plot is for the ECCO-IGS combination. Both plots are for a solution up to degree and order 10 without any smoothing.

areas that the ECCO and IGS data sets should be able to improve upon when combined with GRACE, at least for harmonics at or below degree 10.

4.2 Combinations with GRACE data

Having examined the combination of GPS with OBP, the next step was to examine the contribution of each of these two data sets when they are combined with GRACE. The dense ground-track of GRACE over the course of one month results in relatively low global errors, with only a slight increase over the equator, as shown in Figs 8(a) and (b). Nonetheless, the results shown in Fig. 5 imply that the addition of either GPS or OBP data should improve the accuracy of the final solution. As already mentioned, this improvement is due to the fact that the combination is performed in a least-squares sense, and that parts of the added data sets have predicted errors that are less than those estimated for GRACE. Fig. 6 shows the contribution of either GPS or OBP to the combination with GRACE for the various cases. At first glance, it is clear that OBP contributes overall much more to the combination than GPS, a similar conclusion to that reached previously when only GPS and OBP were combined. The primary influence of GPS lies at the low degrees, in particular the $C_{2,0}$ zonal coefficient. This can also be seen when looking at the percentage improvement of the formal error by each data set (see Fig. 6), as computed using eq. (11). The influence of the GPS data increases as the cases progress from the real to ideal scenarios. This highlights the fact that although the GPS data may have a smaller overall role, it can still provide valuable information to complement GRACE. The same conclusion can also be reached for the OBP data, which shows obvious benefits in a combination solution.

The resonance at order 15 in the GRACE solution is clearly visible in all plots of the contribution and improvement of the formal error, by the distinct stripe feature starting at the 15th tesseral. This is a known feature of the CSR RL04 solutions (Gunter *et al.* 2006) and can even be seen in the degree variances of Fig. 2; so, it is not an artefact caused by the inclusion of either the GPS or OBP data sets. In fact, by the increase in both contribution and improvement in formal error, we see that the introduction of either GPS or OBP helps to stabilize the determination of these resonant coefficients.

It is also interesting to note that the observability of the tesseral coefficients increases with the addition of the OBP data and, to a much lesser extent, with the addition of the GPS data. The near-polar orbit of GRACE results in these tesseral coefficients being one of the more weakly determined coefficients from GRACE. Similar to the improvement seen with the first resonance terms, the OBP data appears to provide sufficient information to make the estimate of the tesseral parameters less uncertain. Again, for GPS this holds only for the lower degrees.

Comparing the contribution with the improvement of the formal error can in some instances provide extra insight into the models used. If large correlations exist within the individual data sets, formal errors of a single coefficient may improve significantly even if the direct contribution to this coefficient according to eq. (10) are small. This effect is clearly visible for the order 15 coefficients, indicating that the resonance also introduces correlations with other coefficients.

The formal errors for the local parameters discussed in Section 2.3 can also be estimated, with the results shown in Table 1. Improvement to the local parameters comes from the correlation of these parameters with the global parameters. For OBP and GPS, this means a correlation between the very low degrees and the higher degrees. For the ideal scenarios, the improvements to the local parameters are negligible, as these distributions cause little correlation between the coefficients. But for the semi-ideal and real cases, the improvements can be large because the gaps introduce correlations between the coefficients. The improvement of the formal error of the degree 1 coefficients is one such example. This coefficient is determined entirely by the OBP and GPS data, but its formal error improves when the GRACE data is included in the combination. This indicates that GRACE helps to improve the estimates of the very low degrees by stabilizing the estimation of the mid and higher degrees.

So far, the performance criteria for the combination solutions has only involved the contribution and formal error improvements of the individual coefficients. This alone is not always sufficient, or intuitive enough, if the geographical (i.e. spatial) distribution of the errors in these solutions is to be examined. To address this issue, the various combined solutions were also evaluated over a number of major ocean and river basins. Using (12), the same error improvement statistics could be computed, but with the results limited to specified regions. The regions chosen represent the major regions of water mass transport across the globe. In addition, their range of geographical location should give insight into which areas can be most improved by the incorporation of GPS and OBP data.

The improvement of the average over the different oceans by combining GRACE with GPS or OBP are given in Table 2. It is clear from the table that GPS can improve the average over the oceans, due to the large improvement of the $C_{2,0}$ coefficient. When the influence of the $C_{2,0}$ coefficient is removed, GPS can still provide an improvement of about 10 per cent. For the combination with

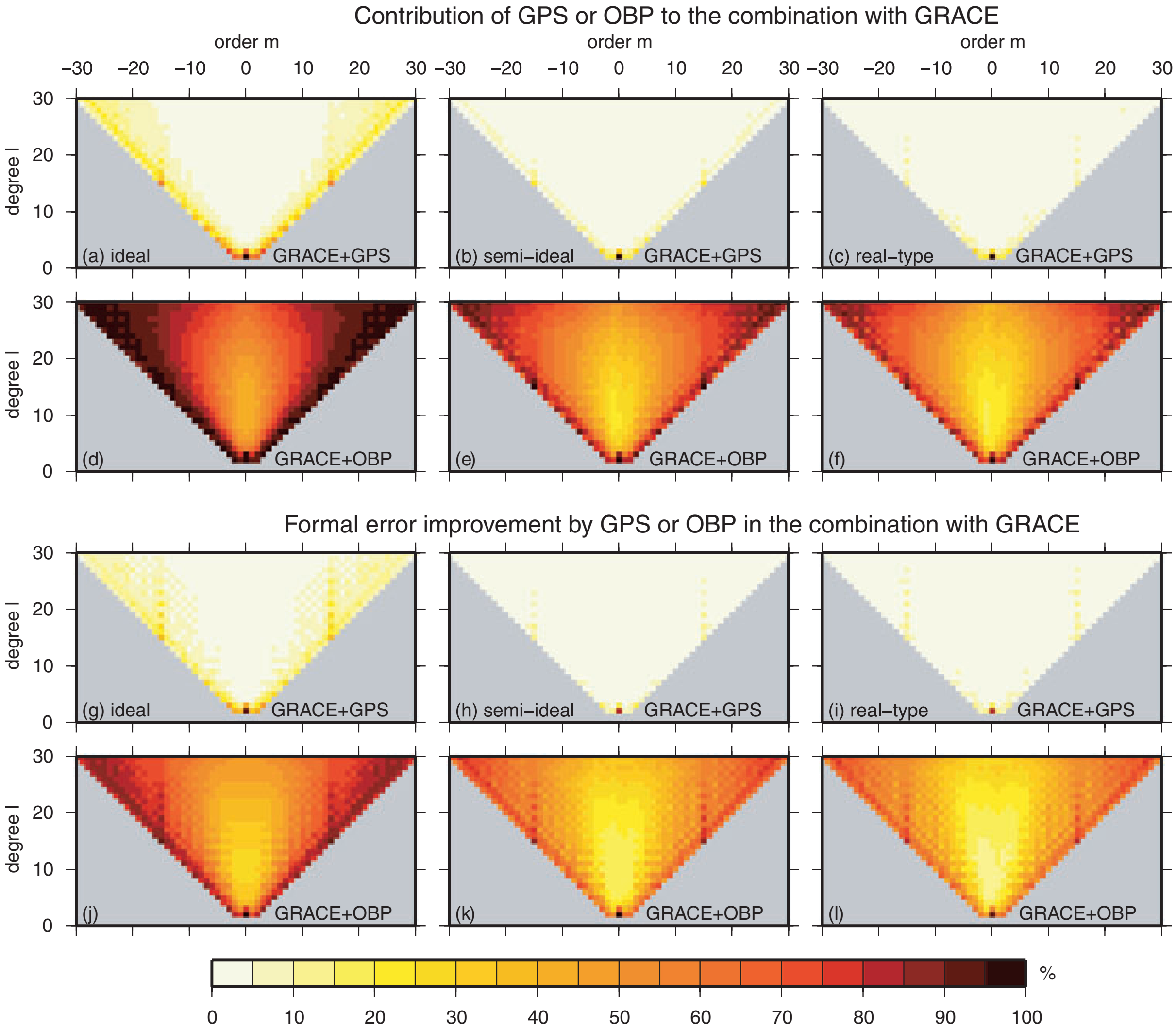

Figure 6. The contribution of GPS or OBP to a combination with GRACE (2006 August) and the formal error improvement by GPS or OBP in the combination with GRACE for the three scenarios. The top two rows show the contribution plots, and the bottom two rows show the formal error improvements. GRACE is combined with GPS (1st and 3rd row) or OBP (2nd and 4th row). The columns give the different scenarios ideal, semi-ideal and real-type from left- to right-hand side. The triangle plots represent the spherical harmonic coefficients, where positive orders are for the cosine coefficients and negative orders are for the sine coefficients.

Table 1. Percentage improvement of formal errors for several low degree parameters from different combinations of GRACE, GPS and OBP. The data sets or combinations of data sets that were used as the reference are shown in brackets. For example, for the formal improvement of $C_{2,0}$, GRACE has been used as the reference for all combinations; but for the degree 1 coefficients, the references are OBP or GPS when they are combined with GRACE, and OBP + GPS for the triple combination.

	GRACE + GPS			GRACE + OBP			GRACE + OBP + GPS		
	Ideal	Semi-ideal	Real-type	Ideal	Semi-ideal	Real-type	Ideal	Semi-ideal	Real-type
l_{max}	7	7	7	10	10	10	12	12	12
					[OBP] + GRACE			[OBP] + GRACE + GPS	
$C_{0,0}$	–	–	–	0.2	69.0	81.1	0.3	85.0	91.8
		[GPS] + GRACE			[OBP] + GRACE			[OBP+GPS] + GRACE	
$C_{1,0}$	0.5	65.6	51.1	0.3	75.3	84.3	0.3	33.8	49.5
$C_{1,1}$	0.5	80.5	49.3	0.2	21.4	59.8	0.2	20.6	54.7
$S_{1,1}$	0.5	78.8	54.4	0.2	72.4	83.7	0.2	25.3	47.4
		[GRACE] + GPS			[GRACE] + OBP			[GRACE] + OBP + GPS	
$C_{2,0}$	91.6	83.8	80.8	97.3	96.2	94.8	97.5	96.3	95.1

Table 2. Formal error improvements in percentage of several ocean means for different combinations of GRACE, GPS and OBP. For all the cases the GRACE solution is taken as a reference. The combinations are done up to degree and order 30 and are smoothed with a Gaussian filter of 500 km. For the percentages after the slash the effect of the $C_{2,0}$ is removed.

	GRACE + GPS			GRACE + OBP			GRACE + OBP + GPS		
	Ideal	Semi-ideal	Real-type	Ideal	Semi-ideal	Real-type	Ideal	Semi-ideal	Real-type
Arctic Ocean	87.7/34.0	79.7/15.8	78.9/15.3	95.2/70.3	93.3/58.9	89.5/46.5	95.3/70.9	93.6/60.6	90.4/50.0
North Atlantic	41.1/35.3	28.6/21.7	22.9/14.9	77.1/74.8	53.7/49.0	49.2/44.2	77.7/75.5	58.7/54.6	53.4/48.7
South Atlantic	38.9/32.0	16.0/7.7	16.1/8.1	75.9/73.1	65.1/61.2	62.9/58.7	76.5/73.9	67.2/63.5	64.4/60.5
Indian Ocean	65.2/38.2	49.6/7.2	48.6/9.5	86.5/75.9	78.5/61.2	76.1/56.0	87.0/76.7	80.7/65.4	77.4/58.5
North Pacific	77.8/35.6	68.4/15.6	67.5/13.3	91.0/73.3	85.5/56.4	82.6/51.5	91.3/74.2	86.7/60.0	83.9/54.7
South Pacific	70.7/36.2	56.7/10.3	54.7/9.9	88.7/75.1	84.1/65.7	82.5/60.9	89.1/75.9	85.2/67.9	83.3/63.1
Southern Ocean	89.1/34.0	81.6/15.3	77.2/13.6	95.7/68.0	94.1/61.2	93.4/56.1	95.8/68.5	94.4/62.4	93.7/57.7
Total	71.8/18.6	65.7/7.0	63.7/7.6	88.1/65.0	81.0/43.5	79.6/38.5	88.3/65.6	82.0/46.6	80.5/41.8

Table 3. Formal error improvements in percentage of several regional averages for different combinations of GRACE, GPS and OBP. For all cases the GRACE solution is taken as a reference. The combinations are done up to degree and order 30 and are smoothed with a Gaussian filter of 500 km. For the percentages after the slash the effect of the $C_{2,0}$ is removed.

	GRACE + GPS			GRACE + OBP			GRACE + OBP + GPS		
	Ideal	Semi-ideal	Real-type	Ideal	Semi-ideal	Real-type	Ideal	Semi-ideal	Real-type
Greenland	78.1/14.8	72.5/7.5	71.3/6.8	89.6/57.5	85.6/42.8	80.3/26.1	89.7/57.9	86.0/44.1	81.2/28.5
Ob	66.4/12.9	62.6/6.6	61.2/6.2	83.6/56.9	73.8/30.8	72.2/26.1	83.8/57.4	74.8/33.4	73.2/28.7
Mississippi	28.3/17.2	17.8/6.4	18.4/7.4	66.0/60.7	37.9/28.3	34.3/24.0	66.4/61.1	41.1/31.9	36.9/27.1
Congo	65.1/15.9	58.6/5.1	57.1/4.6	83.6/60.0	77.5/45.8	76.1/43.4	83.7/60.3	78.4/47.7	76.8/44.3
Amazon	69.4/19.7	62.7/6.1	60.2/5.1	85.6/61.5	79.6/46.5	78.4/43.6	85.8/62.0	80.5/48.8	79.0/45.0
Australia	50.4/24.6	40.6/10.2	37.3/7.5	78.3/66.9	70.1/54.9	67.9/51.1	78.6/67.3	71.7/57.2	68.7/52.4
Antarctica	87.7/33.0	80.4/15.2	75.9/13.4	95.0/68.0	91.9/53.7	91.5/49.2	95.1/68.6	92.3/55.2	91.7/50.9

OBP, a much larger improvement is expected and observed. Here the improvement of the $C_{2,0}$ coefficient is still clearly the dominant effect, but also, the higher degrees now play a role. An overall improvement of about 50 per cent is still observed even after the effect of $C_{2,0}$ is removed, showing that the ECCO model is contributing a significant amount to the combined solution with GRACE.

The improvement over land regions, seen in Table 3, shows a similar picture. The $C_{2,0}$ coefficient is, for both OBP and GPS, the main contributor for the improvement; however, removing the effect of $C_{2,0}$ still leaves a reasonable improvement that can be attributed to GPS and OBP. In general, the improvements are lower than observed for the oceans, due partly to the smaller sizes of the regions. The region of Antarctica is the biggest beneficiary of the additional data, showing improvements of 13 per cent with IGS data and 49 per cent with ECCO even after neglecting the effects of $C_{2,0}$.

In summary, the regional averages provide further support for the benefit of adding GPS and OBP data to GRACE to improve the time variable signal below degree 30. Double digit improvements are seen in nearly all cases, with some areas such as the Southern Ocean and Antarctica seeing improvements of over 90 per cent when $C_{2,0}$ is considered. The spatial differences are interesting to note, as it appears to indicate that certain regions, mostly in the higher latitudes, seem to benefit the most from the combination solutions. The exact reasons for this are currently being explored.

4.3 The final combination: GRACE, GPS and OBP

The final step of the sensitivity study was to combine all three data sets into a single solution. From the results of the previous subsections, it was expected that GPS would play a minor role in this combination, with improvements mainly limited to the lower degrees, that is, through to degrees 4–6. More substantial contributions were expected from the incorporation of OBP data, with possible improvements up to degree and order 30. We recall that this limit for the OBP data was caused by both the quality of the data and the grid spacing used in the simulation. The 5° spacing of the gridded data results in a resonance at the 36th order, and causes instability in the solution. As a result, for the triple combination, the maximum degree was set to 30 for the three data sets.

In Fig. 7, the degree error variances of the various different combinations are shown, including the triple combination of GRACE, GPS and OBP. For comparison, a GRACE only curve is provided together with the hydrology degree power spectrum signal generated from the Land Dynamics(LaD) 'Fraser' model (Milly & Shmakin 2002). To highlight the most realistic scenarios tested, only the real and semi-ideal cases are shown in the figure.

Overall, the results show that the introduction of any of the data sets improves the formal standard deviation. On average, the triple combinations show a factor 2–5 improvement of the formal errors when compared with a GRACE-only solution. In particular, the combination of GRACE with the semi-ideal OBP and GPS shows the lowest overall errors through degree 30. The change in formal errors, in terms of degree variances, when switching from the (irregular) real-data network to the semi-ideal (i.e. homogeneous distribution of points) for GPS and OBP is fairly small. Furthermore, the addition of real-type GPS to the combination of GRACE and real-type OBP only shows a small effect on the lower degrees, but a large improvement on degree 2 when combined with GRACE alone. As expected, the improvements upon the GRACE-only solution are dominated by the OBP data.

By looking at the intersection of the LaD curve and that of any of the triple combinations, Fig. 7 suggests that the addition of the new data sets to GRACE shifts the observable hydrology signal (where signal dominates noise) from degree 15 to approximately

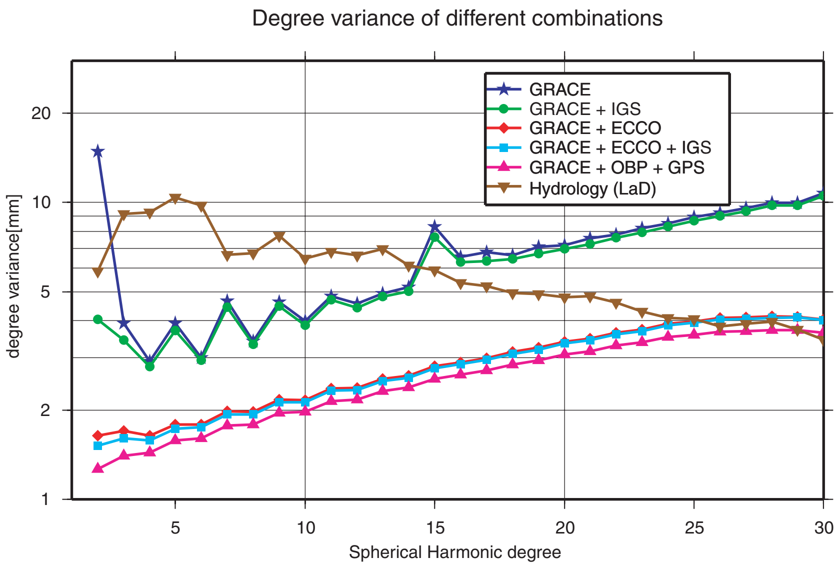

Figure 7. Degree variance plot of the surface loads resulting from different combinations. For this plot, GRACE was combined with, real-type IGS(green), real-type ECCO(red), real-type IGS-ECCO(magenta) and semi-homogeneous GPS-OBP(cyan). Also the variance of the hydrology signal is shown(brown), for which the LaD model 'Fraser' was used. The degree variances are given in equivalent water height in (mm).

degree 25, that is, an increase in spatial resolution (half-width) from ∼1300 to ∼800 km. The increase in both spatial resolution and signal accuracy is encouraging for future work.

Other important points highlighted by Fig. 7 are the improvements at the low degrees and the smoothing of the resonances. The real-data triple combination shows an order of magnitude improvement in the degree two coefficients, and the instability in the GRACE-only solutions below degree 10 is substantially attenuated with the addition of the GPS and OBP data. The spike at degree 15, caused by the first-order resonance, is also eliminated.

To visualize the improvements gained by adding the real-type GPS and OBP data sets to GRACE, Fig. 8 shows the total global errors of the solution in terms of equivalent water height, using both the 2006 August and 2004 September CSR RL04 solutions for comparison. The strength of each data set in combination with GRACE is nicely illustrated, and the improvement between the GRACE-only errors and those of the final combination is clearly visible. In particular, the improvements to the September 2004 solution is notable and once again emphasizes how the GPS and OBP data sets can substantially improve not only good quality GRACE solutions, but also those solutions whose accuracy has been reduced due to a near-repeat ground-track pattern. The figure also shows how the triple combination could be further improved. For example, the regions of highest error in Figs 8(g) and (h), such as Africa, South America and Russia, are those in which the IGS network has the fewest number of stations. The results of the simulations imply that adding more stations to these regions could help to reduce the uncertainties in the triple combinations by 1–2 cm.

The last three columns of Table 1 contain the improvement in the local parameters and the $C_{2,0}$ coefficient for the triple combinations. When comparing these results with the other results given in the table, it is clear that the triple combination has an advantage over them. This is evidenced by the slightly higher improvement in the $C_{0,0}$ and $C_{2,0}$ coefficients with respect to other combinations. For the degree 1 terms, a peak improvement of nearly 50 per cent is seen for the real-type triple combination. Note that for the degree 1 terms, the triple combination uses the OBP-GPS derived degree 1 terms as reference for the percentage improvement, as opposed to degree 1 terms obtained from GPS or OBP only. This explains why the percentage improvement appears lower than the degree 1 terms of the other columns in Table 1. This result is still impressive considering that GRACE is not directly sensitive to degree 1 harmonics, but only influences their determination through correlations with higher degree terms.

Looking at the regional comparisons in Tables 2 and 3, the triple combinations show a small gain in improvement over the other combinations in the table. This fact is not completely due to the improvement of the $C_{2,0}$ coefficient, as double digit improvements are also observed when $C_{2,0}$ is neglected. One other interesting observation from Table 3 is that the Mississippi basin appears to be less affected by the improved $C_{2,0}$ coefficient than the other basins, presumably due to its geographical location. This makes the Mississippi basin a nice subject for future analysis.

5 CONCLUSIONS

A series of simulations have been conducted to examine the influence that the combination of GPS and/or modelled OBP data has with GRACE data. A number of variables went into the solutions, including the distribution of data points, the assigned errors and the maximum degree and order of the solution. As such, both ideal and realistic cases were explored to see their differences. The final solutions were evaluated using a range of statistical metrics showing the contribution of each data set down to the level of individual harmonic coefficients.

The main conclusions of the sensitivity study was that the addition of either GPS or OBP data to GRACE would help improve the stability and accuracy of the estimated global mass redistribution. In general, the OBP models show the largest contribution mostly due to their low errors and dense distribution of gridpoints; however, it was also made clear that the inclusion of GPS was important for the determination of the low degree harmonics, in particular $C_{2,0}$.

An additional benefit of including either GPS or OBP into the GRACE solutions is the ability to estimate the degree one

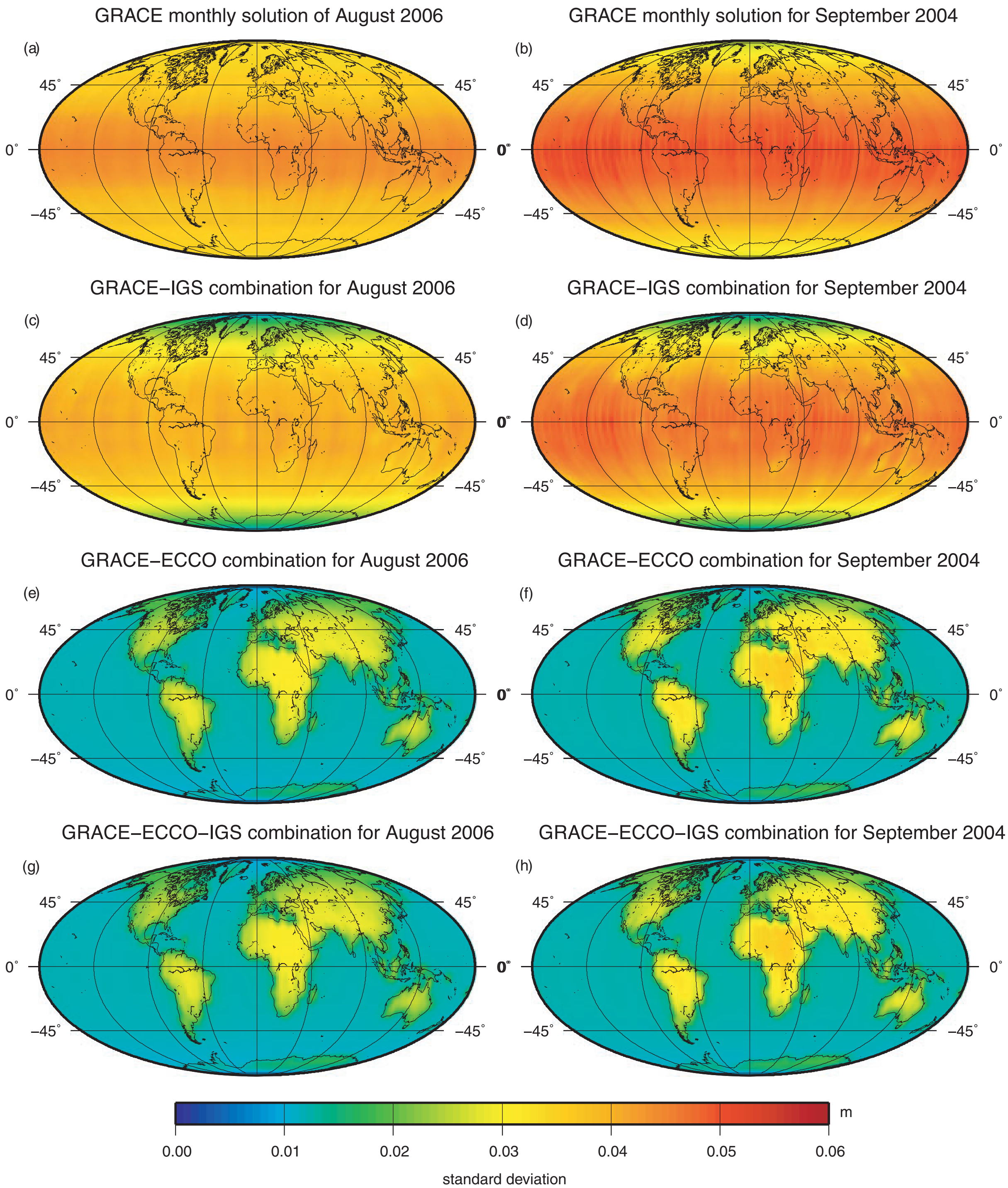

Figure 8. Standard deviation of GRACE and GRACE combined with IGS and/or ECCO projected on the globe. The top panel gives the two GRACE-only solutions used in this study, that is, for 2006 August (a) and 2004 September (b). The second row shows the combination of these two GRACE solutions with IGS (c and d). The next row shows the combination of these two GRACE solutions with ECCO (e and f). The bottom row gives the triple combination for these two months (g and h). For all plates the maximum degree of the solution is 30 and no smoothing is performed.

coefficients (i.e. geocentre motion). In fact, the accurate estimation of the higher degree coefficients by GRACE enabled the more accurate determination of the degree 1 coefficients, presumably through reduction of omission and commission errors.

As mentioned in Section 1, one of the primary objectives of these simulations was to lay the foundation for future combinations using real data. This study showed that, given the likely error characteristics of the IGS data and ECCO models, a combined solution to degree and order 30 can be estimated, which is 2–5 times more accurate than a solution based only on GRACE data. Additionally, improvements to both $C_{2,0}$ and the first-order resonances are gained, and the solution was extended to include degree one coefficients. There are a number of other considerations that need to be made when working with real data, but the general conclusions obtained from these simulations were valuable in establishing the initial guidelines for future combinations.

ACKNOWLEDGMENTS

The authors would like to thank the University of Texas at Austin Center for Space Research for providing the two RL04 covariance matrices used in this study.

MJFJ thanks the Nederlandse Organisatie voor Wetenschappelijk Onderzoek (NWO), Aard- en Levenswetenschappen (ALW) division for providing additional support for the study and reference grant number ALW1PJ/07011.

JK acknowledges support provided by the German Research Foundation (DFG) under grant KU 1207/6-1, within the Special Priority Program SPP 1257 Mass Transport and Mass Distribution in the System Earth.

REFERENCES

Blewitt, G., 2003. Self-consistency in reference frames, geocenter definition, and surface loading of the solid Earth, *J. geophys. Res.,* **108**(B2), 2103, doi:10.1029/2002JB002082.

Blewitt, G. & Clarke, P., 2003. Inversion of Earth's changing shape to weigh sea level in static equilibrium with surface mass redistribution, *J. geophys. Res.,* **108**(B6), 2311, doi:10.1029/2002JB002290.

Chambers, D.P., Tamisica, M.E., Nerem, S.R., & Ries, J.C., 2007. Effects of ice melting on GRACE observations of ocean mass trends, *Geophys. Res. Lett*., **39,** L05610, doi:10.1029/2006GL029171.

Clarke, P.J., Lavalleé, D.A., Blewitt, G., van Dam, T.M. & Wahr, J.M., 2005. Effect of gravitational consistency and mass conservation on seasonal surface mass loading models, *Geophys. Res. Lett.,* **32**(8), L08306, doi:10.1029/2005GL022441.

Dong, D., Dickey, J.O., Chao, Y. & Cheng, M.K., 1997. Geocenter variations caused by atmosphere, ocean and surface ground water, *Geophys. Res. Lett.,* **24**(15), 1876–1870.

Farrell, W.E., 1972. Deformation of the Earth by surface loads, *Rev. Geophys.*, **10**(3), 761–797.

Fukumori, I., Raghunath, R., Fu, L.-L. & Chao, Y., 1999. Assimilation of TOPEX/Poseidon altimeter data into a global ocean circulation model: how good are the results?, *J. geophys. Res.,* **104**(C11), 25 647–25 665.

Gunter, B.C., Ries, J., Bettadpur, S. & Tapley, B., 2006. A simulation study of the errors of omission and commission for GRACE RL01 gravity fields, *J. Geodesy,* **80**(7), 341–357.

Klokočnik, J., Wagner, C.A., Kostelecký, J., Bezděk, A., Novák, P. & McAdoo, D., 2008. Variations in the accuracy of gravity recovery due to ground track variability: GRACE, CHAMP, and GOCE, *J. Geodesy,* **82**(12), 917–927.

Kusche, J. & Schrama, E.J.O., 2005. Surface mass redistribution inversion from global GPS deformation and GRACE gravity data, *J. geophys. Res.,* **110**, B09409, doi:10.1029/2004JB003556.

Lavallée, D., van Dam, T., Blewitt, G. & Clarke, P., 2006. Geocenter motion from GPS: A unified observation model, *J. geophys. Res.,* **111,** B05405, doi:10.1029/2005JB003784.

Mendes Cerveira, P.J., Hobiger, T., Weber, R. & Schuh, H., 2006. Spatial spectral inversion of the changing geometry of the Earth from SOPAC GPS data, in *Dynamic Planet: Proceedings of IAG Symposium,* Vol. 130, pp. 194–201, Springer, Berlin.

Métivier, L., Greff-Lefftz, M. & Diament, M., 2005. A new approach to computing accurate gravity time variations for a realistic earth model with lateral heterogeneities, *Geophys. J. Int.,* **162,** 570–574.

Milly, P.C.D. & Shmakin, A.B., 2002. Global modeling of land water and energy balances, 1: the land dynamics (LaD) model, *J. Hydrometeor.,* **3,** 283–299.

Munekane, H., 2007. Ocean mass variations from GRACE and tsunami gauges, *J. geophys. Res.,* **112**, B07403, doi:10.1029/2006JB004618.

Ponte, R.M., Wunsch, C. & Stammer, D., 2007. Spatial mapping of time-variable errors in Jason-1 and TOPEX/Poseidon sea surface height measurements, *J. Atmos. Oceanic Technol.,* **24,** 1078–1085.

Reigber, C., 1989. Gravity field recovery from satellite data, in *Theory of Satellite Geodesy and Gravity Field Determination, Lecture Notes in Earth Sciences Series,* Vol. 25, Springer, Berlin.

Stammer, D., Wunsch, C., Fukumori, I. & Marshall, J., 2002. State estimation improves prospects for ocean research, *Eos, Trans. AGU,* **83**(27), 289.

Swenson, S., Chambers, D. & Wahr, J., 2008. Estimating geocenter variations from a combination of GRACE and ocean model output, *J. geophys. Res.,* **113**, B08410, doi:10.1029/2007JB005338.

Tapley, B.D., Bettadpur, S., Ries, J.C., Thompson, P.F. & Watkins, M.M., 2004. GRACE measurements of mass variability in the Earth system, *Science,* **305**(5683), 503–505.

Wahr, J.M., Molenaar, M. & Bryan, F., 1998. Time variablility of the earth's gravity field: hydrological and oceanic effects and their possible detection using grace, *J. geophys. Res.,* **103**(B12), 30 205–30 229.

Wu, X., Argus, D.F., Helfin, M.B., Ivins, E.R. & Webb, F.H., 2002. Site distribution and aliasing effects in the inversion for load coefficients and geocenter motion from GPS data., *Geophys. Res. Lett.,* **29**(24), doi:10.1029/2002GL016324.

Wu, X., Heflin, M.B., Ivins, E.R. & Fukumori, I., 2006. Seasonal and inter-annual global surface mass variations from multisatellite geodetic data, *J. geophys. Res.* **111**, B09401, doi:10.1029/2005JB004100.